Further Development of Oxley's Predictive Force Model for Orthogonal Cutting

Article *in* Machining Science and Technology · February 2015

DOI: 10.1080/10910344.2014.991026

3 authors, including:

Erme Chen
UNSW Australia
4 PUBLICATIONS **3** CITATIONS
SEE PROFILE

Huaizhong Li
Griffith University
71 PUBLICATIONS **600** CITATIONS
SEE PROFILE

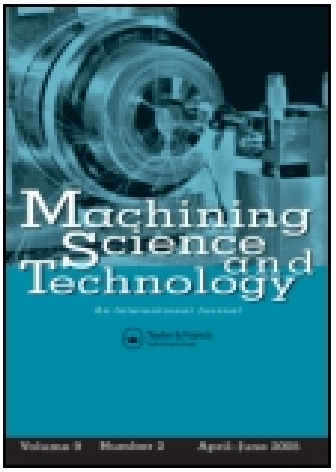

Machining Science and Technology: An International Journal

Publication details, including instructions for authors and subscription information:
http://www.tandfonline.com/loi/lmst20

Further Development of Oxley's Predictive Force Model for Orthogonal Cutting

Yun Chen[a], Huaizhong Li[ab] & Jun Wang[a]

[a] School of Mechanical and Manufacturing Engineering, The University of New South Wales, Sydney, Australia

[b] Griffith School of Engineering, Gold Coast Campus, Griffith University, Nathan, Australia

Published online: 09 Feb 2015.

To cite this article: Yun Chen, Huaizhong Li & Jun Wang (2015) Further Development of Oxley's Predictive Force Model for Orthogonal Cutting, Machining Science and Technology: An International Journal, 19:1, 86-111, DOI: 10.1080/10910344.2014.991026

To link to this article: http://dx.doi.org/10.1080/10910344.2014.991026

Machining Science and Technology, 19:86–111

ISSN: 1091-0344 print /1532-2483 online
DOI: 10.1080/10910344.2014.991026

Taylor & Francis
Taylor & Francis Group

FURTHER DEVELOPMENT OF OXLEY'S PREDICTIVE FORCE MODEL FOR ORTHOGONAL CUTTING

Yun Chen[1], Huaizhong Li[1,2], and Jun Wang[1]
[1]*School of Mechanical and Manufacturing Engineering, The University of New South Wales, Sydney, Australia*
[2]*Griffith School of Engineering, Gold Coast Campus, Griffith University, Nathan, Australia*

□ *An analytical modelling approach based on Oxley's predictive machining theory is presented to evaluate the cutting forces, chip thickness and temperature distributions in the orthogonal cutting process. In this approach, the work material properties are modelled using the Johnson–Cook constitutive material law, which represents the flow stress of the material as a function of strain, strain rate, and temperature. For the determination of the tool-chip interface temperature, an evenly distributed rectangular heat source near the cutting edge is used instead of a plane heat source. The tool thermal model is simplified by neglecting the temperature variations along the tool-chip interface to avoid the high cost of computation time. Finite difference method is applied for solution of the thermal model. The performance of the developed model is validated with the experimental data in machining of steel* 1045. *A comparison of the outputs from Oxley's original model and the modified model is provided. The model is further assessed by using two other materials,* Al 6086-T6 *and* Ti6Al4V. *Close agreements with experimental results have been shown.*

Keywords cutting force model, chip thickness, constitutive material law, orthogonal cutting, Oxley's machining theory, temperature distribution

INTRODUCTION

Metal cutting is a complex process involving a multitude of phenomena such as plasticity, friction, heat generation, heat flow, etc. Work material is severely deformed and sheared in the cutting process, specifically, at high deformation rates and temperatures. The increased deformation rates and temperatures greatly influence the cutting process in terms of the plastic deformation in the shear plane and the interaction between the tool and chip. There has been extensive study to understand the metal cutting

Address correspondence to Huaizhong Li, Griffith School of Engineering, Gold Coast Campus, Griffith University, Nathan, QLD 4222, Australia. E-mail: lihuaizhong@gmail.com; h.li@griffith.edu.au.

Color versions of one or more of the figures in the article can be found online at www.tandfonline.com/lmst.

process, and different models have been developed. Ernst and Merchant (1941) introduced the early shear plane model which determines the shear angle by minimum energy. Lee and Shaffer's (1951) slip-line field model applied rigid plasticity analysis to orthogonal cutting. However, the above two models are only valid for an idealized rigid-perfectly plastic work material. The parallel-sided shear zone theory proposed by Oxley (1989) enhanced the material model, considering the effect of strain, strain rate and temperature on the material flow stress to predict the shear angle, cutting forces and other outputs of interest.

Oxley (1989) used piecewise, high-order curve fitting equations to represent the relationship of flow stress and strain-hardening index as functions of the velocity-modified temperature and carbon content for a range of plain carbon steels. Unfortunately, a documented representation of the relationship is available only for a few metals, mainly low carbon steels. Further development of such a material model for aluminium alloys has been presented by Bao and Stevenson (1976) and Kristyanto et al. (2002). However, for a wide range of other engineering materials, there are no such available equations that can be used as the inputs for Oxley's predictive machining theory (Li and Wang, 2012), which is one of the main restrictions for further application of Oxley's theory. In recent years, an extensive amount of constitutive models of material properties at high strains, high strain rates, and high temperatures have been established and applied to metal cutting.

Adibi-Sedeh et al. (2003) modified Oxley's theory by using different material models, including the Johnson–Cook material model, the history-dependent power law material model, and the mechanical threshold stress model, to simulate the orthogonal cutting process for several materials. It is found that the Johnson–Cook model performs the best in the prediction of cutting forces. Lalwani et al. (2009) used the Johnson–Cook material model, instead of Oxley's original material model, to predict temperatures and cutting forces in orthogonal cutting. Li and Wang (2012) employed the Johnson–Cook material model to determine the flow stress of Inconel 718.

As the flow stress of the material is temperature dependent, determination of the temperature in the deformation zones is crucial in modelling the metal cutting process. Komanduri and Hou (2001) proposed a thermal model of the metal cutting process by utilising a moving band heat source for the primary and secondary zones. This model has been integrated into Oxley's predictive theory for force prediction by Karpat and Ozel (2005). Huang and Liang (2003) utilized Oxley's theory for orthogonal cutting process with modifications of the thermal model similar to Komanduri and Hou, considering the thermal properties of CBN tools. Plane heat source has been assumed in the thermal modelling in the work by Komanduri and Hou (2001) and Huang and Liang (2003).

According to Tay (1993; 1976), the plane heat source is not accurate, as the actual heat flow in the region of the tool rake face is a combination of a

distributed heat source due to chip plastic deformation, a plane heat source due to friction along the tool-chip interface, and a plane heat sink due to heat conduction into the tool. Little information is available on the actual distribution of heat generation rate in metal cutting (Boothroyd, 1963; Tay, 1993). Tay et al. (1976) assumed a distributed heat source in the secondary zone based on experimental observations to determine the temperature fields in metal cutting. Boothroyd (1963) used a rectangular heat source in the chip near the cutting edge to simulate the temperature distribution and found that it gave reasonable results.

The aim of this article is to further develop Oxley's theory by extending its applicability to more materials by using the Johnson-Cook material model and an analytical thermal method based on Tlusty's work (2000). This thermal method transforms the two-dimensional steady-state problem into a single-dimensional transient one, based on the assumption that the mass transfer of heat along the chip velocity direction is much more powerful than heat conduction in the same direction. Instead of the plane heat source due to friction, an evenly distributed rectangular heat source in the secondary zone is employed. A simulation of orthogonal cutting for three materials namely steel, aluminium and titanium alloys is conducted. The predicted forces, chip thicknesses and temperature fields are then compared with the experimental data to verify the proposed model.

MODEL DEVELOPMENT

Oxley's Theory

Oxley's theory is based on a model of chip formation derived from the slip-line field analysis and the strain rate analysis of experimental flow fields. Plain strain and steady-state conditions are assumed and the tool is taken to be perfectly sharp, as shown in Figure 1. The plane *AB*, near the centre of the primary shear zone, and the tool-chip interface are assumed to be the directions of maximum shear stress and maximum shear strain rate. Two parameters C_0 and δ are introduced for the analysis of the strain rates in the primary and secondary zones as in Figure 1b. C_0 represents the relative length of the primary shear zone with respect to the thickness of the primary shear zone and δ is the ratio of the thickness of the secondary shear zone to the chip thickness.The foundation of this theory is that the resultant forces R transmitted by the shear plane *AB* and the tool-chip interface are in equilibrium. Therefore, the shear angle ϕ in the plane *AB* and the parameters C_0 and δ can be determined by analysing the stress distributions along the plane *AB* and the tool-chip interface.

In the primary zone, Oxley (1989) assumed the strain rate along *AB* as a function of C_0, and the strain at *AB* as a half of the average strain in the

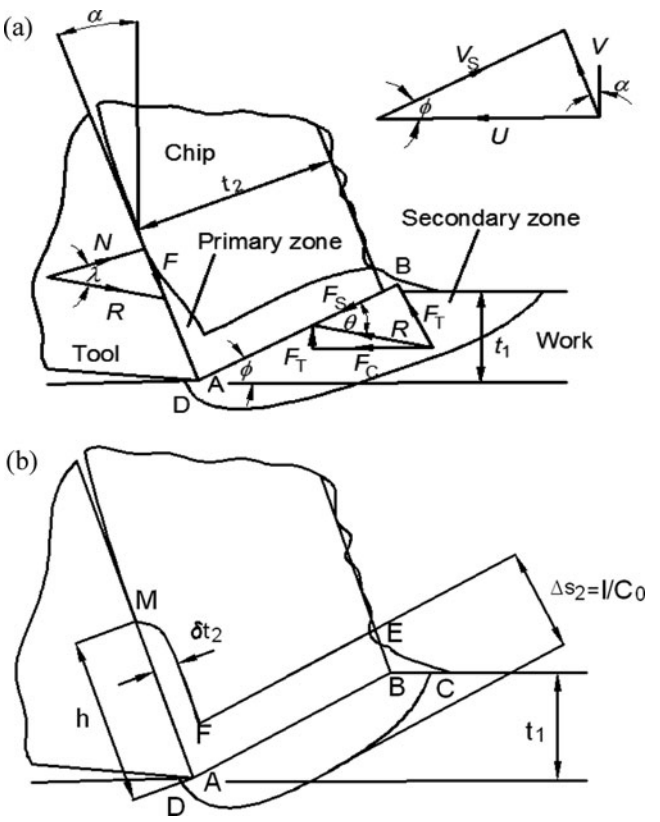

FIGURE 1 Chip formation model for orthogonal machining (a) deformation zone with force and velocity vectors; (b) simplified deformation zone.

primary zone, based on experimental observations. The temperature at *AB* is derived from the plastic work in the primary zone with the consideration that a proportion of the total work $F_s V_s$ is conducted into the work material. The strain rate, strain and temperature are then used to determine the equivalent flow stress k_{AB} according to the material model upon the velocity-modified temperature and carbon content. Once C_0 and ϕ are determined, the shear force F_s, the angle θ which is made by R with AB, and the mean friction angle λ in Figure 1, and other outputs of interest, can be evaluated.

However, to satisfy the force equilibrium, the results of C_0 and ϕ are not always reasonable. Therefore, another parameter δ has been used to investigate the stress and strain distribution at the tool-chip interface. The strain rate and temperature along the interface can be derived from several empirical equations as a function of δ. The equivalent flow stress k_{chip} at the interface is calculated with the strain rate and temperature, neglecting the influence of the strain. The outputs from both the primary and secondary zone are compared to check the equilibrium. The shear stress τ_{int} at the tool-chip interface derived from the primary shear zone analysis and k_{chip} from

the secondary zone should be equal when the sticking friction is assumed over the interface.

As a result, the shear angle ϕ is determined by the above requirement. From the slip-line analysis, the normal stress σ'_N at the boundary point B can be represented in terms of C_0 and material properties. Assuming uniform distribution of normal stress along the tool-chip interface, the average normal stress σ_N can also be obtained by the normal force N which is one output from the plane AB analysis. Similar to the shear stress along the interface, σ'_N and σ_N should be equal so that C_0 can then be determined. The last unknown parameter δ is found from minimum work considerations. The values of C_0 and δ found in this way have been shown to be in good agreement with experimental results.

Material Model

It is important to establish the relation between the process parameters and the strength of the deforming material for the development of machining process models. The constitutive model of Johnson and Cook (1983) is for materials subjected to large strains, high strain rates and high temperatures that are similar to the conditions in metal cutting. The material constants in the model can be obtained from torsion tests over a wide range of strain rates, static tensile tests, dynamic Hopkinson bar tests and Hopkinson bar tests at elevated temperatures. The Johnson–Cook constitutive relation has been widely used for analysing high strain rate deformation of metals. It provides an empirical relationship for the flow stress σ of a material as

$$\sigma = (A + B\varepsilon^n)\left(1 + C\ln\left(\frac{\dot{\varepsilon}}{\dot{\varepsilon}_0}\right)\right)\left(1 - \left(\frac{T - T_r}{T_m - T_r}\right)^m\right) \tag{1}$$

where ε, $\dot{\varepsilon}$, and $\dot{\varepsilon}_0$ are the equivalent strain, equivalent strain rate, and reference strain rate (usually 1 s^{-1}), respectively. T is the instantaneous temperature of the material, T_r is the reference temperature and T_m is the melting temperature. A, B, C, n, and m are constants obtained by material tests. Table 1 shows the constants for *AISI 1045*, *Al 6082-T6* and *Ti6Al4V*.

Shear Flow Stress in the Primary Zone

Since the cutting process is assumed to be a plain strain condition, according to the Von Mises criterion, the equivalent shear stress k_{AB} at AB by using the Johnson–Cook model can be expressed as

$$k_{AB} = \frac{1}{\sqrt{3}}\left(A + B\varepsilon_{AB}^n\right)\left(1 + C\ln\left(\frac{\dot{\varepsilon}_{AB}}{\dot{\varepsilon}_0}\right)\right)\left(1 - \left(\frac{T_{AB} - T_r}{T_m - T_r}\right)^m\right) \tag{2}$$

TABLE 1 Johnson–Cook Model Parameters for Different Materials

Material	T_m (°C)	A (MPa)	B (MPa)	C	n	m
AISI 1045[1]	1460	553.1	600.8	0.0134	0.234	1
Al 6086-T6[2]	582	250	243.6	0.00747	0.17	1.31
Ti6Al4V[3]	1630	862.5	331.2	0.012	0.34	0.8

[1]Constants from Jaspers and Dautzenberg (2002).
[2]Constants from Adibi-Sedeh and Madhavan (2002).
[3]Constants from Meyer and Kleponis (2001).

where k_{AB}, $\dot{\varepsilon}_{AB}$, and ε_{AB} are the equivalent shear flow stress, equivalent strain rate and strain, and T_{AB} is the average temperature at AB. According to Oxley (1989), $\dot{\varepsilon}_{AB}$ and ε_{AB} are considered constant and can be expressed as

$$\dot{\varepsilon}_{AB} = \frac{\dot{\gamma}_{AB}}{\sqrt{3}} = C_0 \frac{V_s}{\sqrt{3}l} \tag{3}$$

$$\varepsilon_{AB} = \frac{\gamma_{AB}}{\sqrt{3}} = \frac{\cos\alpha}{2\sqrt{3}\cos(\phi - \alpha)\sin\phi} \tag{4}$$

where $\dot{\gamma}_{AB}$ and γ_{AB} are the maximum shear strain rate and strain at AB, respectively, l is the length of AB, ϕ is the shear angle, and α is the rake angle as shown in Figure 1. V_S is the shear velocity, which can be calculated from the cutting velocity U using the equation

$$V_s = \frac{\cos\alpha}{\cos(\phi - \alpha)} U \tag{5}$$

The temperature at AB is determined by considering the plastic work done in the primary shear zone, and is expressed as

$$T_{AB} = T_r + \eta \frac{1-\beta}{\rho S t_1 w} \frac{F_s \cos\alpha}{\cos(\phi - \alpha)} \tag{6}$$

where the second term on the right-hand side is the temperature rise at AB due to the shear plastic deformation, β is the proportion of heat conducted into the work material, the factor η $(0 < \eta \leq 1)$ is used to scale the average temperature rise to compensate the fact that not all of the plastic work of chip formation has occurred at AB, ρ and S are the density and specific heat of the work material respectively, t_1 is the uncut chip thickness, and w is the depth of cut.

A non-dimensional thermal number R_T is introduced, i.e.,

$$R_T = \frac{\rho S U t_1}{K} \tag{7}$$

where K is the thermal conductivity of the work material. An empirical estimation of β (Oxley, 1989) is given as

$$\beta = 0.5 - 0.35\log_{10}(R_T \tan\phi) \quad \text{for } 0.04 \le R_T \tan\phi \le 10.0 \tag{8a}$$

$$\beta = 0.3 - 0.15\log_{10}(R_T \tan\phi) \quad \text{for } R_T \tan\phi > 10.0 \tag{8b}$$

Assuming k_{AB} as the average equivalent shear flow stress in the primary zone, the shear force F_s can be evaluated from

$$F_s = \frac{k_{AB} t_1 w}{\sin\phi} \tag{9}$$

Thereafter, once C_0 and ϕ are set, k_{AB} and F_s can be evaluated by using Equations (2–9) iteratively.

By considering the stress equilibrium equation along AB (Oxley, 1989), there exists the relationship of

$$p_A - p_B = \frac{\Delta k}{\Delta s_2} l \tag{10}$$

where p_A and p_B are the hydrostatic (mean compressive) stresses at point A and B, Δk is the shear strength difference in primary shear zone, Δs_2 is the width of the primary zone. Due to the adoption of Johnson–Cook constitutive model, $\Delta k/\Delta s_2$ becomes (see Appendix),

$$\frac{\Delta k}{\Delta s_2} = C_0 \frac{2k_{AB} n B \varepsilon_{AB}^n}{(A + B\varepsilon_{AB}^n) l} \tag{11}$$

The angle θ between the resultant force R and line AB in Figure 1, and the normal stress σ'_N at point A should therefore be modified as

$$\theta = \tan^{-1}\left(1 + 2\left(\frac{\pi}{4} - \phi\right) - C_0 \frac{n B \varepsilon_{AB}^n}{A + B\varepsilon_{AB}^n}\right) \tag{12}$$

$$\sigma'_N = k_{AB}\left(1 + \frac{\pi}{2} - 2\alpha - 2C_0 \frac{n B \varepsilon_{AB}^n}{A + B\varepsilon_{AB}^n}\right) \tag{13}$$

Shear Flow Stress at the Tool-Chip Interface

The shear flow stress k_{chip} at the tool-chip interface is determined using the Johnson–Cook model and the Von Mises criterion, i.e.,

$$k_{chip} = \frac{1}{\sqrt{3}}\left(A + B\varepsilon_{\text{int}}^{n}\right)\left(1 + C\ln\left(\frac{\dot{\varepsilon}_{\text{int}}}{\dot{\varepsilon}_0}\right)\right)\left(1 - \left(\frac{T_{\text{int}} - T_r}{T_m - T_r}\right)^{m}\right) \tag{14}$$

where $\dot{\varepsilon}_{\text{int}}$ and ε_{int} are the maximum equivalent shear strain rate and shear strain at the tool-chip interface respectively, and T_{int} is the average temperature at the interface. According to Oxley (1989), $\dot{\varepsilon}_{\text{int}}$ and ε_{int} are assumed constant along the interface, and can be estimated from

$$\dot{\varepsilon}_{\text{int}} = \frac{\dot{\gamma}_{\text{int}}}{\sqrt{3}} = \frac{V}{\sqrt{3}\delta t_2} \tag{15}$$

$$\varepsilon_{\text{int}} = \frac{\gamma_{\text{int}}}{\sqrt{3}} = \frac{h}{\sqrt{3}\delta t_2} \tag{16}$$

where $\dot{\gamma}_{\text{int}}$ andγ_{int} are the maximum shear strain rate and shear strain at the interface, t_2 is the chip thickness, h is the tool-chip contact length, and V is the rigid chip velocity. t_2 and V can be calculated according to the geometric relations given by

$$t_2 = \frac{t_1\cos(\phi - \alpha)}{\sin\phi} \tag{17}$$

$$V = \frac{U\cos\phi}{\cos(\phi - \alpha)} \tag{18}$$

and h is given by (see Appendix)

$$h = \frac{t_1\sin\theta}{\cos\lambda\sin\phi}\left\{1 + \frac{C_0\frac{nB\varepsilon_{AB}^{n}}{A+B\varepsilon_{AB}^{n}}}{3\left[1 + 2(\frac{\pi}{4} - \phi) - C_0\frac{nB\varepsilon_{AB}^{n}}{A+B\varepsilon_{AB}^{n}}\right]}\right\} \tag{19}$$

where the friction angle λ satisfies the following equation

$$\lambda = \theta - \phi + \alpha \tag{20}$$

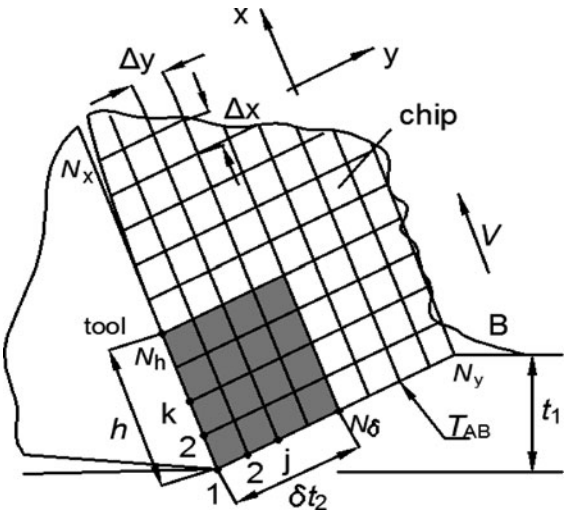

FIGURE 2 Illustration of the finite difference method for the temperature field in the chip.

Temperature at the Tool-Chip Interface

The heat transfer equation governing the temperature distribution in the chip is given by (Lazoglu and Altintas, 2002)

$$\frac{\partial^2 T_c}{\partial x^2} + \frac{\partial^2 T_c}{\partial y^2} + \frac{\dot{q}}{K} = \frac{\rho S}{K}\frac{\partial T_c}{\partial t} \tag{21a}$$

where T_c is the chip temperature field, $\dot{q}$ is the instantaneous rate of heat generation per unit volume, t is time, and x, y are positions in the chip velocity direction and the direction parallel to line AB respectively. As stated before, mass transfer in the x direction is much more powerful than conduction in the same direction. Then Equation (21a) thus becomes

$$\frac{\partial^2 T_c}{\partial y^2} + \frac{\dot{q}}{K} = \frac{\rho S}{K}\frac{\partial T_c}{\partial t} = \frac{\rho S}{K} V \frac{\partial T_c}{\partial x} \tag{21b}$$

In the above equation, it is noted that $\partial T_c/\partial t$ can be replaced by $V\partial T_c/\partial x$. To solve this partial differential equation, a finite difference method is used as introduced by Tlusty (2000). Figure 2 shows that the chip geometry is meshed into small discrete elements. For each nodal point (j, k) of the chip, the partial differentials in Equation (21b) can then be approximated as

$$\frac{\partial^2 T_c}{\partial y^2} = \frac{T_{c(j+1,k)} + T_{c(j-1,k)} - 2T_{c(j,k)}}{\Delta y^2} \tag{22}$$

$$\frac{\partial T_c}{\partial x} \cong \frac{T_{c(j,k+1)} - T_{c(j,k)}}{\Delta x} \tag{23}$$

A plane heat source along the tool-chip interface was employed by Tlusty (2000). To improve the accuracy, the plane heat source is replaced by an evenly distributed rectangular heat source in the secondary zone (Boothroyd, 1963). Therefore, the heat generation rate $\dot{q}$ in Equation (21b) for each node (j, k) in the secondary zone becomes

$$\dot{q}_{(j,k)} = \frac{\dot{Q}_c - \dot{Q}_t}{\delta t_2 h w} \quad \text{for } 1 \le k \le N_h \text{ and } 1 \le j \le N_\delta \tag{24a}$$

$$\dot{q}_{(j,k)} = 0 \quad \text{for } N_x > k > N_h \text{ or } N_y > j > N_\delta \tag{24b}$$

where $\dot{Q}_c$ is the total heat generated in the secondary zone, $\dot{Q}_t$ is the total heat rate escaping from the tool, N_h and N_δ are the numbers of grids for the secondary zone along the x and y axis respectively, and N_x and N_y are the maximum numbers of grids for the chip in the x and y axis respectively. $\dot{Q}_c$ is the product of the friction force F and the chip velocity V, i.e.,

$$\dot{Q}_c = FV \tag{25}$$

From the vector diagram in Figure 1, F can be represented as

$$F = \frac{F_s}{\cos\theta} \sin\lambda \tag{26}$$

Substituting Equations (22–26) into Equation (21b), the thermal balance equation for each node in a differential form is

$$\frac{T_{c(j+1,k)} + T_{c(j-1,k)} - 2T_{c(j,k)}}{\Delta y^2} + \frac{\dot{q}_{(j,k)}}{K} = \frac{\rho S}{K} V \frac{T_{c(j,k+1)} - T_{c(j,k)}}{\Delta x} \tag{27}$$

To determine the heat $\dot{Q}_t$ escaping from the tool, Tlusty (2000) has simplified the shape of the tool and the thermal field in it. The tool is modelled as a wedge with the tool-chip interface at the flat top and the slope of the tool wedge is 45°, as shown in Figure 3. The isotherms of the tool are more or less the lines of equal distance from the cutting zone. The tool as a wedge with the tool-chip contact at the flat top and the bottom is at room temperature T_r. The tool is divided into slices with the thickness Δz, width b_i, and depth w (into the paper). The thermal field is assumed single-dimensional in z direction, and every slice has a constant temperature throughout. The slope sides of the tool wedge are assumed to be

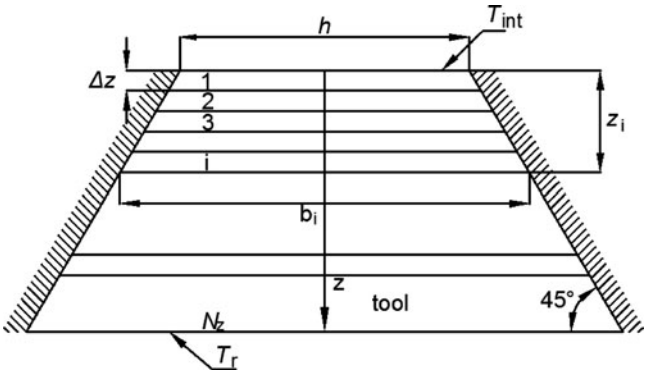

FIGURE 3 Illustration of the finite difference method for the temperature field in the tool.

isolated, that is, all heat entering a slice leaves it with the same power $\dot{Q}_t$ flowing through the tool in the steady state. According to such a simplification of the tool thermal field, the temperature along the tool-chip contact length should also be constant and the average temperature at the interface has been used as the temperature at the flat top of the tool wedge

$$T_{\text{int}} = \frac{1}{N_h} \sum_{1}^{N_h} T_{c(1,k)} \tag{28}$$

The thermal field of the tool wedge simplified by Tlusty has neglected the temperature variation along the tool-chip interface, resulting in a very low cost of the computation time. In contrary, in the models by Komanduri and Hou (2001) and Lazoglu and Altintas (2002), complex and time-consuming iterative approaches have to be used to guarantee equal temperature distributions at the contact interface on both the chip and tool sides.

According to Fourier's heat conduction law, the total heat conduction rate $\dot{Q}_t$ at the ith slice can be expressed as

$$\dot{Q}_t = -K_a b_i w \frac{\partial T_t}{\partial z} \tag{29a}$$

where T_t is the tool temperature field and K_a is the thermal conductivity of the tool. The depth w of each slice is considered to be constant and equal to the width of cut, but in fact when the heat flows from one slice to the next one along the z direction, the heat also transforms along the direction of the depth, w. Such an approximation is supposed to underestimate the heat escaping from the tool. The preceding equation can be approximated using

the finite difference method, i.e.,

$$\dot{Q}_t = -K_a w \frac{T_{t(i+1)} - T_{t(i)}}{R_i} \tag{29b}$$

with $R_i = \Delta z / b_i$. Denoting $r = \sum_1^{N_z} \frac{R_i}{K_a}$ and adding Equation (29b) for all slices yields

$$\dot{Q}_t = (T_{\text{int}} - T_r) \frac{w}{r} \tag{30}$$

The temperature distribution in the chip and the total heat conduction rate $\dot{Q}_t$ from the tool are not known initially. Therefore, an iterative process is needed for the computation. In the chip temperature field, the boundary conditions are vital to calculate the temperature distributions. T_{AB} at the shear plane AB is taken as one of the boundary conditions and the heat convected from the chip into the surrounding air is assumed negligible. Additionally, the temperatures for the tool and chip at the interface should be equal, which means that $T_{c(j-1,k)}$ is equal to $T_{c(j,k)}$ in Equation (27) for the lowest element, $j = 1$. An initial value can be assigned for the heat rate $\dot{Q}_t$ escaping from the tool. The tool and chip temperature fields can be determined based on the initial assignment of $\dot{Q}_t$.

After solving Equation (27) for each node in the chip temperature field and Equation (30) for the tool, T_{int} and a new $\dot{Q}_t$ can be obtained. This new $\dot{Q}_t$ is then used to re-calculate T_{int}. If the two T_{int} are almost equal, iterations for calculation of the temperature distributions end. A flow chart to determine $T_{c(j,k)}$ and $\dot{Q}_t$ is given in Figure 4. T_{int} is the final output to compute k_{chip}. In this calculation, the thermal conductivities of the tool and the workpiece and the specific heat capacity of the workpiece are thought to be constant, although they dependent on the temperature.

Model Integration

To obtain cutting forces and other outputs, the Johnson-Cook material model and the temperature field model are integrated into Oxley's analytical theory. There are three unknown parameters of importance in the above analysis, i.e., ϕ, C_0 and δ. An iteration calculation approach is employed to find them, as shown in Figure 5. Assuming that only sticking friction occurs over the tool-chip interface, the average shear stress at the interface is found from the equation

$$\tau_{\text{int}} = \frac{F}{hw} \tag{31}$$

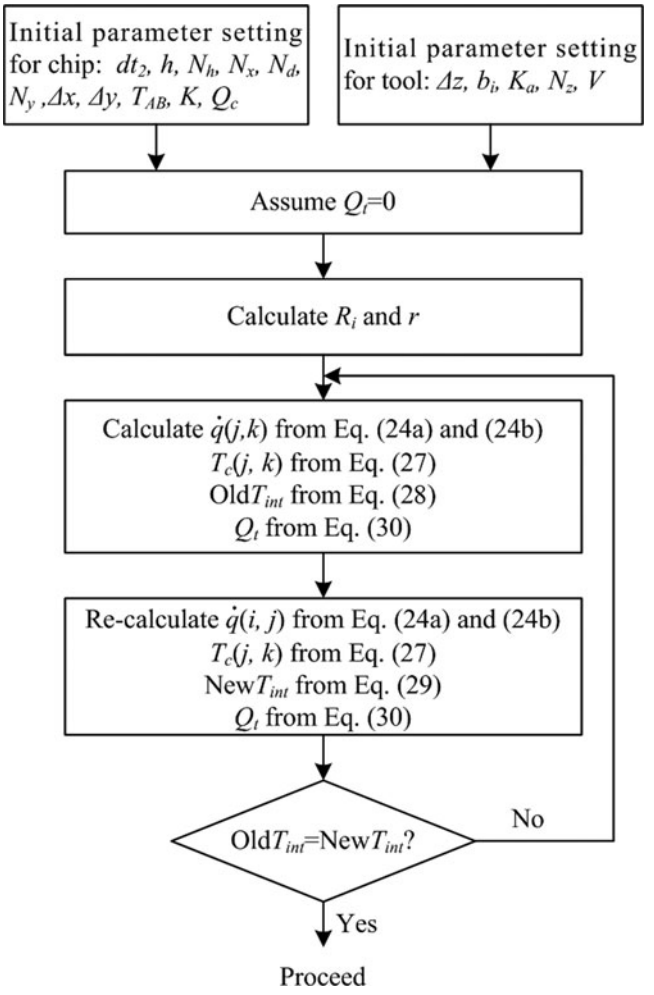

FIGURE 4 Flow chart for solving the tool-chip interface temperature.

The shear angle ϕ is then determined by the fact that k_{chip} as a function of strain-rate, strain and temperature should be equal to τ_{int}. If there is not only one ϕ which makes τ_{int} and k_{chip} equal, the highest ϕ is chosen. Further assuming a uniform normal stress distribution along the tool-chip interface, the average normal stress at the interface is then given by

$$\sigma_N = \frac{N}{hw} \tag{32}$$

where N is the normal force at the interface and can be calculated by

$$N = \frac{F_s}{\cos\theta}\cos\lambda \tag{33}$$

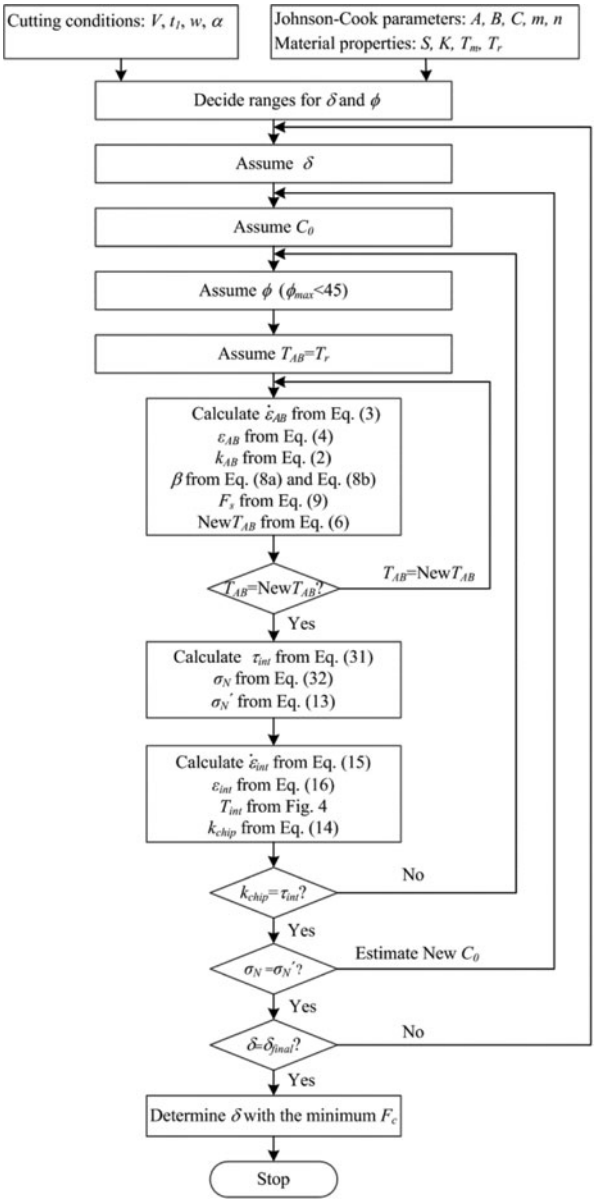

FIGURE 5 Flow chart of cutting force simulation.

To achieve the equilibrium, the average normal stress σ_N from Equation (32) should be equal to σ_N' as a function of C_0 from Equation (13). As shown in Figure 5, a new estimated C_0 from the equation that follows is used

$$C_0 = \frac{A + B\varepsilon_{AB}^n}{2nB\varepsilon_{AB}^n}\left[1 + \frac{\pi}{2} - 2\alpha - \frac{\sigma_N}{k_{AB}}\right] \tag{34}$$

TABLE 2 Cutting Conditions and Some Computed Results ($w = 1.6$ mm)

Test	U (m/min)	α (deg)	t_1 (um)	$C_0{}^1$	$T_{AB}{}^1$ (°C)	$C_0{}^2$	$T_{AB}{}^2$ (°C)	$C_0{}^3$	$T_{AB}{}^3$ (°C)
1	200	−7	150	6.09	382	7.86	376	7.9	322
2	200	5	150	5.51	422	7.16	434	6.6	266
3	200	−7	300	5.92	294	8.02	285	7.3	306
4	200	5	300	4.49	277	5.99	285	5.4	245
5	300	−7	150	5.91	399	7.48	398	7.9	319
6	300	5	150	4.71	304	6.74	335	6.3	277
7	300	−7	300	5.49	347	7.12	345	7.3	308
8	300	5	300	4.6	257	6.59	275	5	238

[1]Model 1; [2]Model 2; [3]Mode 3.

The iterations end until the difference between σ_N and σ'_N is insignificant, and then C_0 is determined. The last unknown δ is obtained from the minimum work principle, which means to take the value of δ when F_C is the minimum.

MODEL VERIFICATION

The developed model has been implemented using Matlab codes. To verify the proposed model, three work materials, namely steel 1045, aluminium alloy *Al 6082-T6* and titanium alloy *Ti6Al4V*, are considered. The results are presented as follows.

Steel 1045

The experimental data used was published by Ivester et al. (2000) for orthogonal cutting of steel *AISI 1045*. The cutting conditions are given in Table 2. Simulations of the modified model are performed using constant work material properties, with conductivity, density, and specific heat capacity of 51.9 W/(m·K), 7862 kg/m^3 and 486 J/(kg°C), respectively. Constant tool conductivity of 40 W/(m·K) is used for all tests. For the finite difference solution of the thermal model, N_h, N_x, N_y and N_z are set to 200, 400, 20 and 40, respectively, and the tool wedge reaches the ambient temperature at $z = 5t_2$.

To understand the effect of the proposed thermal model on force predictions and other outputs, results obtained from the modified models are compared to that obtained using Oxley's original model. Predictions with different models and the experimental data are shown in Figure 6. Hereafter the modified Oxley's model with the proposed thermal model and Johnson–Cook material model is referred to as model 1. Model 2 uses Oxley's original material model and the new thermal model, and model 3 is Oxley's original model. It can be seen that the predicted results obtained by different models are of the same order of magnitude as the experimental

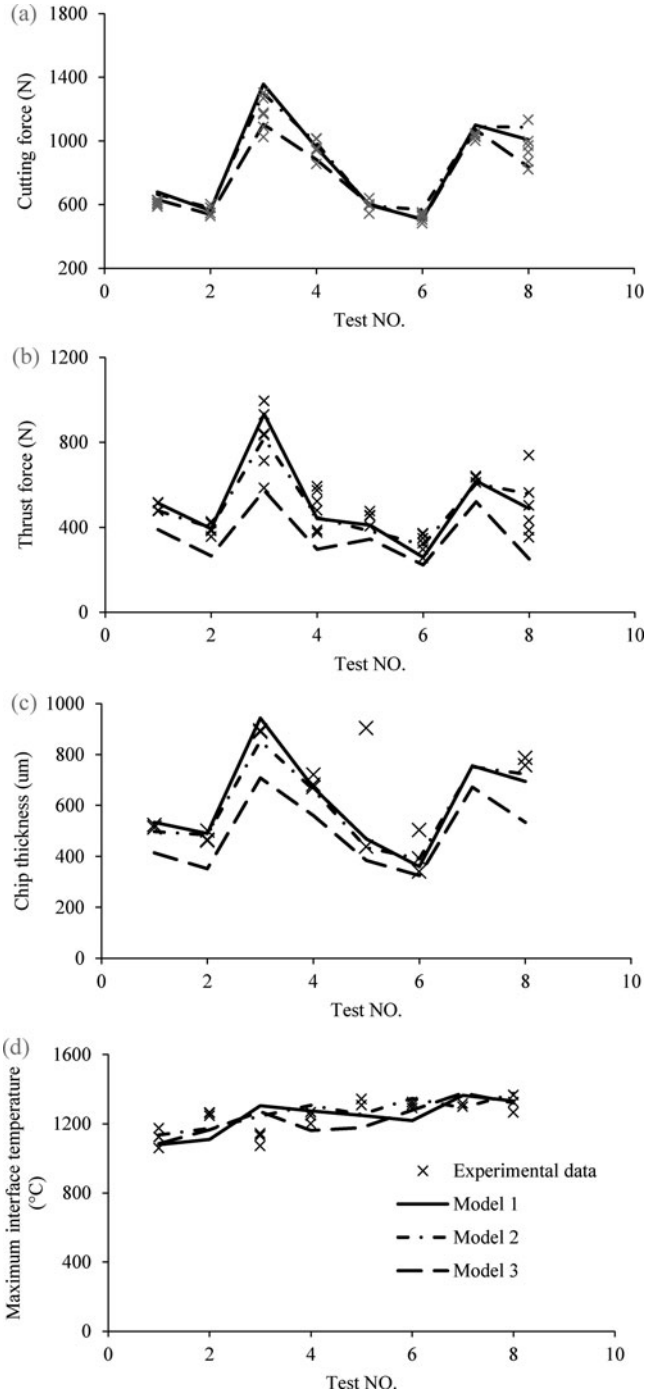

FIGURE 6 Comparison of different models (a) cutting force; (b) thrust force; (c) chip thickness; and (d) maximum tool-chip interface temperature.

data. Figures 6a and 6b show that model 1 predicts the largest force values in most cases, while model 3 predicts the smallest. The same trend can also be observed in Figure 6c in the prediction of the chip thickness, where model 3 underestimates it. The reason that model 2 differs from Oxley's original model (model 3) is due to the combination of the enhanced temperature model and the use of constant thermal properties for the workpiece and tool.

A comparison of the predicted maximum tool-chip interface temperatures and the calibrated experimental temperatures by Adibi-Sedeh and Madhavan (2002, 2003) is given in Figure 6d, which shows a good agreement. As can be seen, the maximum tool-chip interface temperature is sensitive to the increase of the cutting speed. Both the experimental and predicted temperatures in tests 5–8 are higher than those in tests 1–4, respectively. The temperature distributions for the chip in test 1 predicted by model 1 and model 2 are shown in Figure 7. The maximum tool-chip interface temperature predicted by model 2 is larger than that by model 1. The temperature distributions from the two models are similar to the results presented by Karpat and Özel (2005), although the maximum temperature location along the tool-chip interface predicted by Karpat and Özel is closer to the cutting edge than that in Figure 7, due to the use of the uniform heat intensity at the interface.

A summary of some predicted results by different models is presented in Table 2. The predicted results T_{AB} by model 1 and model 2 are close to each other and model 3 predicts the smallest T_{AB}. For the parameter C_0, model 1 gives the smallest values while C_0 obtained from model 2 are close to the values from model 3. Such observations for different models indicate that the material model has a more significant influence on C_0 than the thermal model.

Aluminium Alloy *Al 6082-T6*

Model 1 is also applied to simulate the orthogonal cutting process for aluminium alloy *Al 6082-T6*. The experimental results were presented by Jaspers (1999), where the *Al 6082-T6* tube workpiece was machined under dry condition with a wall thickness of 4 mm. The test conditions are listed in Table 3. The workpiece properties are considered to be independent of the temperature with workpiece conductivity, density, and specific heat capacity of 170 W/(m·K), 2700 kg/m^3 and 894 J/(kg°C), respectively. Tool conductivity of 40 W/(m·K) is constant for all tests. For the thermal model, N_h, N_x, N_y and N_z are set to 200, 400, 20 and 40 respectively, and the tool wedge reaches the ambient temperature at $z = 5t_2$.

A comparison of the simulated and experimental results is shown in Figure 8. The variations of cutting force F_c and thrust force F_t versus the cutting speed under two different chip thicknesses are illustrated in Figures

TABLE 3 Cutting Conditions and Some Computed Results ($w = 4$ mm, $\alpha = 6$ deg)

Test	U (m/min)	t_1 (mm)	C_0	T_{int} (°C)
1	2	0.2	7.23	287
2	4	0.2	6.38	318
3	6	0.2	5.83	336
4	8	0.2	5.55	394
5	2	0.4	6.34	326
6	4	0.4	5.51	391
7	6	0.4	5.12	427
8	8	0.4	4.86	440

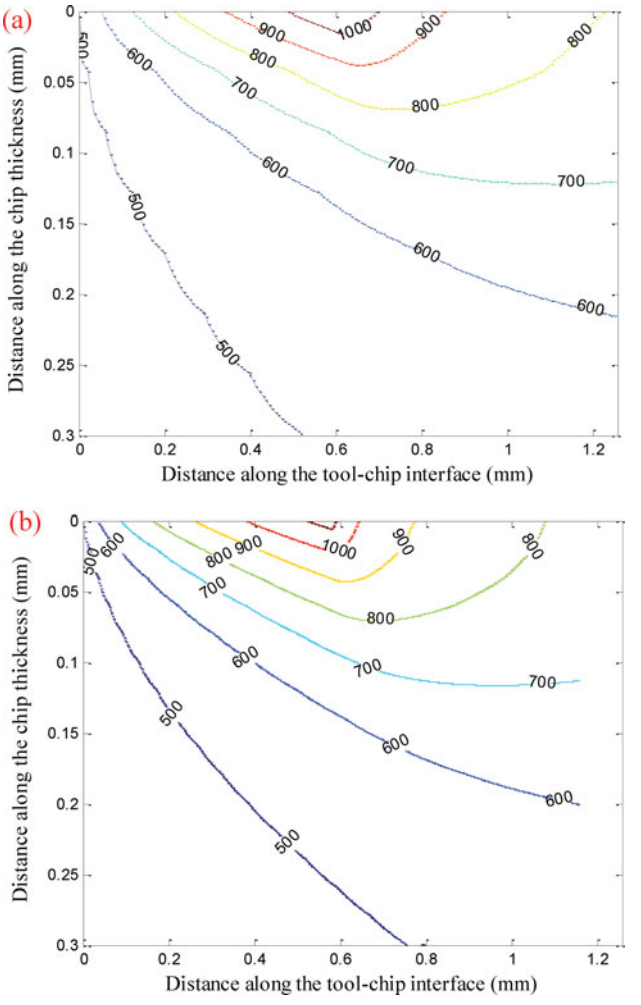

FIGURE 7 Temperature distributions of the chip for *AISI 1045* in test 1 (a) predicted by Model 1 and (b) predicted by Model 2.

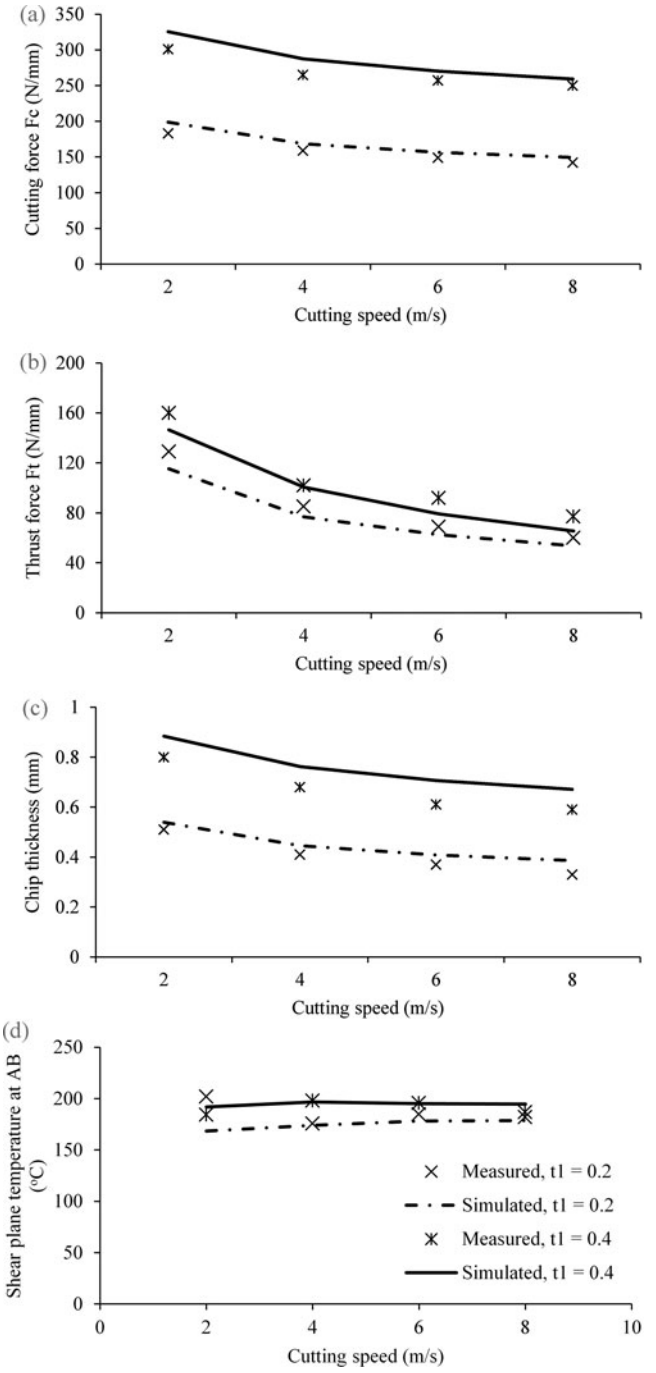

FIGURE 8 Comparison between the simulated and experimental results for cutting an aluminium alloy *Al 6082-T6* (a) Cutting force; (b) thrust force; (c) chip thickness; and (d) shear plane temperature at *AB*.

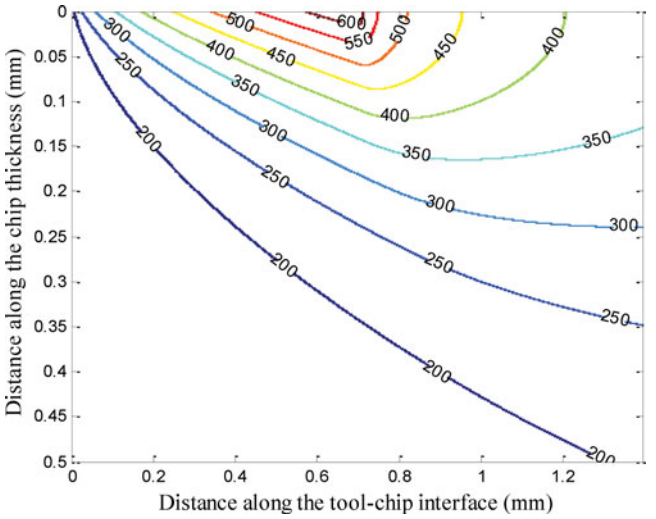

FIGURE 9 Simulated temperature distributions of the chip for Al 6082-T6 (cutting conditions: as listed for test 6 in Table 3).

8a and 8b, respectively. It can be seen that both F_c and F_t decrease along with an increase of the cutting speed, or a decrease of the uncut chip thickness. The maximum predicted force percentage errors are 8.5% and 14.9% for F_c and F_t respectively, which is within a reasonable range. In addition, there is a good agreement in terms of the overall trend. The chip thicknesses also decrease along with an increase of the cutting speed or a decrease of the uncut chip thickness as shown in Figure 8c. The maximum percentage error for the predicted chip thickness is 16.8% at a cutting speed of 4 m/s with an uncut chip thickness 0.2 mm. For $t_1 = 0.4$ mm, this model overestimates the chip thickness.

Figure 8d shows the variation of the shear plane temperature T_{AB} versus the cutting speed and chip thickness. The maximum percentage error for the predicted shear plane temperature is 16.6% at cutting speed 2 m/s and uncut chip thickness 0.2 mm. An increase of the cutting speed seems to have limited influence on the shear plane temperature, as can be seen from both predicted and measured results. On the other hand, the increase of the cutting speed or uncut chip thickness increases the average interface temperature as shown in Table 3. An example of the simulated chip temperature field at cutting speed 4 m/s and uncut chip thickness 0.4 mm is shown in Figure 9.

Titanium Alloy *Ti6Al4V*

A simulation study on orthogonal cutting of titanium alloy *Ti6Al4V* is used to further assess the proposed model 1. The predicted results are compared with the experimental data from Barry et al. (2001) in turning a

TABLE 4 Cutting Conditions and Some Computed Results ($w = 1.1$ mm, $\alpha = -6$ deg, U = 1 m/s)

Test	t_1 (mm)	C_0	T_{AB} (°C)	T_{int} (°C)	T_{AB}[1] (°C)	T_{int}[1] (°C)
1	0.1	4.78	502.3	811	622	890
2	0.08	5.01	502.1	783	657	924
3	0.06	4.95	501.9	736	632	936

[1]Predicted temperatures from Özel and Zeren (2005).

Ti6Al4V disk with a nominal thickness of 1.1 mm (width of cut) and a diameter of 25 mm. The cutting conditions are given in Table 4. According to Sun et al. (2009), chips in machining *Ti6Al4V* at low cutting speeds (below 75 m/min) were continuous, while the plastic deformability became poor at high cutting speed. At a cutting speed of 75 m/min and above, thermoplastic instabilities predominated, which resulted in 100% chip segmentations. These observations were similar to the experimental results by Barry et al. (2001). Therefore, low cutting speed 60 m/min is chosen for simulation. The work material properties are considered to be independent of the temperature, with workpiece conductivity, density, and specific heat capacity as 7.3 W/(m·K), 4430 kg/m^3 and 526.3 J/(kg·C), respectively.

A constant tool conductivity of 40 W/(m·K) is used. N_h, N_x, N_y and N_z are set to 200, 400, 20 and 40, respectively, and the tool wedge reaches the ambient temperature at $z = 5t_2$. The predicted forces are compared against the experimental forces as shown in Figure 10. The maximum prediction errors for F_c and F_t are 8.0% and 11.0%, respectively. The predicted C_0, T_{AB} and T_{int} by the proposed model are listed in Table 4, along with the temperatures predicted by Özel and Zeren (2005). It can be seen that the temperatures at the tool-chip interface predicted by the proposed model showed an increasing trend with the increase of the uncut chip thickness. The predicted temperature field in test 1 is given in Figure 11.

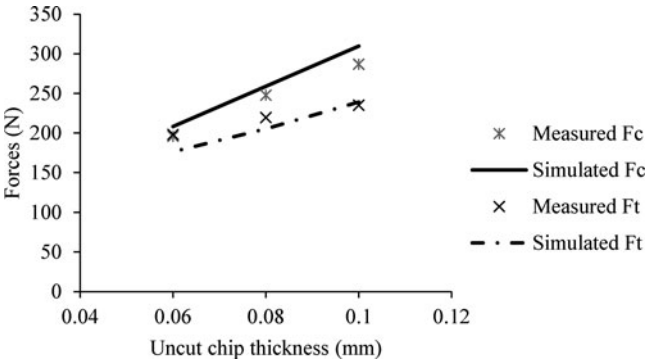

FIGURE 10 Comparison between the simulated and experimental results for cutting titanium alloy *Ti6Al4V*.

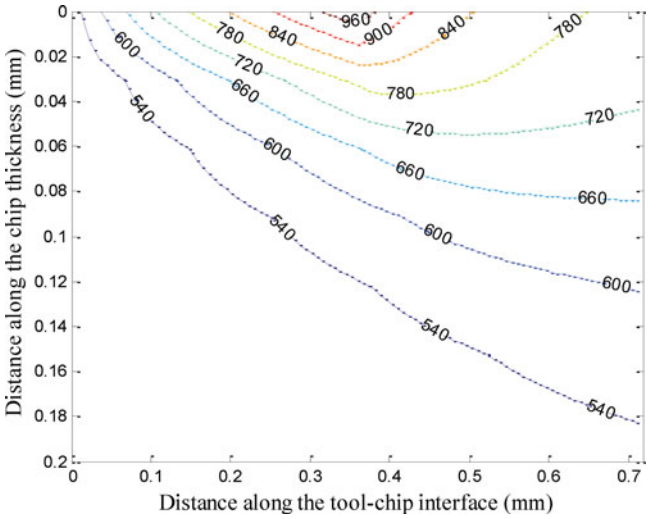

FIGURE 11 Temperature distributions of the chip for *Ti6Al4V* in test 1.

CONCLUSIONS

An analytical cutting force model for orthogonal cutting has been presented by expanding Oxley's predictive machining theory for a broader range of work materials. This has been achieved by integrating Johnson–Cook constitutive material model. Accordingly, the temperature models have also been further developed. An evenly distributed heat source near the cutting edge was used to replace the plane heat source model at the tool-chip interface. Thermal balance equations for both the chip and tool were determined in partial differential forms. The finite difference method was utilized for the solutions of the steady-state tool and chip temperature fields. The developed model has been verified by comparing the predicted cutting force components, chip thickness and temperatures in the primary and secondary zones with the corresponding experimental data or results predicted by other researchers in the literature for steel, aluminium alloy and titanium alloy, in which a good agreement has been demonstrated. The effects of cutting speed, uncut chip thickness and tool rake angles on the cutting force components and chip thickness have been also investigated. The developed model can be extended to oblique cutting or used to develop predictive force models for practical machining operations.

NOMENCLATURE

A	plastic equivalent strain in Johnson-Cook constitutive model
b_i	width of ith slice
B	strain related constant in Johnson-Cook constitutive model

C	strain-rate sensitivity constant in Johnson-Cook constitutive model
C_0	ratio of thickness of primary zone and length of AB
F_s, F, F_c	shear, friction and cutting forces
h	tool-chip interface length
i, j, k	Index numbers in x, y, z directions
k_{AB}, k_{chip}	shear flow stresses of AB and chip
Δk	shear strength difference in primary shear zone
K, K_a	thermal conductivities of work material and tool
l	length of AB
m	thermal softening parameter in Johnson–Cook constitutive model
n	strain-hardening parameter in Johnson–Cook constitutive model
N_x, N_y, N_z	total numbers in x, y, z directions
N_h, N_δ	numbers of interface length and secondary zone thickness
N	normal force
p_A, p_B	hydrostatic pressures at point A and B
$\dot{q}$	instantaneous heat generation rate per unit volume
$\dot{q}_{(i,j)}$	instantaneous heat generation rate for the node (j, k)
$\dot{Q}_c$, $\dot{Q}_t$	total heat generation rate and heat rate escaping from tool
R_T	thermal number
R	resultant force
Δs_2	width of the primary zone
S	specific heat
t_1, t_2	uncut and cut chip thicknesses
T, T_r, T_m	temperature, reference temperature and melting temperature
T_{AB}, T_{int}	temperatures at AB and interface
T_c, T_t	temperatures at the chip and tool
$T_{c(j,k)}$	temperature at (j, k) node of the chip
$T_{t(i)}$	temperature of ith slice of tool
U, V_s, V	cutting, shear and chip velocities
w	width of cut
Δx, Δy	element dimensions in x, y directions
Δz	thickness of slice
α	rake angle
β	proportion of heat conducted into workpiece
δ	ratio of thickness of secondary zone and chip thickness
ε, $\dot{\varepsilon}$, $\dot{\varepsilon}_0$	equivalent strain, equivalent strain rate, and reference strain rate
$\dot{\varepsilon}_{AB}$, ε_{AB}	equivalent strain rate and strain at AB
$\dot{\varepsilon}_{\text{int}}$, ε_{int}	equivalent strain rate and strain at the interface
ϕ	shear angle
$\dot{\gamma}_{AB}$, γ_{AB}	maximum shear strain rate and strain at AB

$\dot{\gamma}_{\text{int}}$, γ_{int}	maximum shear strain rate and strain at interface
η	parameter to scale average temperature rise at AB
λ	friction angle
θ	angle between F_s and R
ρ	density
σ'_N, σ_N	normal stresses at point A and interface
τ_{int}	average shear stress at the interface

REFERENCES

Adibi-Sedeh, A.H.; Madhavan, V. (2002) Effect of some modifications to oxley's machining theory and the applicability of different material models. *Machining Science and Technology: An International Journal*, 6(3): 379–395.

Adibi-Sedeh, A.H.; Madhavan, V.; Bahr, B. (2003) Extension of Oxley's Analysis of Machining to Use Different Material Models. *Journal of Manufacturing Science and Engineering*, 125(4): 656–666.

Bao, H.; Stevenson, M.G. (1976) A basic mechanism for built-up edge formation in machining. *CIRP Annals-Manufacturing Technology*, 25: 53–57.

Barry, J.; Byrne, G.; Lennon, D. (2001) Observations on chip formation and acoustic emission in machining Ti–6Al–4V alloy. *International Journal of Machine Tools and Manufacture*, 41(7): 1055–1070.

Boothroyd, G. (1963) Temperatures in orthogonal metal cutting. *Proceedings of the Institution of Mechanical Engineers*, 177(1): 789–810.

Ernst, H.; Merchant, M.E. (1941) Chip formation, friction, and high quality machined surfaces. *Surface Treatment of Metals (American Society for Metals)*, 29: 299–378.

Huang, Y.; Liang, S.Y. (2003) Cutting forces modeling considering the effect of tool thermal property—application to CBN hard turning. *International Journal of Machine Tools and Manufacture*, 43(3): 307–315.

Ivester, R.W.; Kennedy, M.; Davies, M.; Stevenson, R; Thiele, J.; Furness, R.; Athavale, S. (2000) Assessment of machining models: progress report. *Machining Science and Technology: An International Journal*, 4(3): 511–538.

Jaspers, S.P.F.C. (1999) Metal Cutting Mechanics and Material Behavior, Technische Universiteit Eindhoven, PhD. dissertation, The Netherlands.

Jaspers, S.P.F.C.; Dautzenberg, J.H. (2002) Material behavior in conditions similar to metal cutting: flow stress in the primary shear zone. *Journal of Materials Processing Technology*, 122(2–3): 322–330.

Johnson, G.J.; Cook, W.H. (1983) A constitutive model and data for metals subjected to large strains, high strain rates and high temperatures. *Proceedings of the 7th International Symposium on Ballistics*, 19–21 April, The Hague, The Nerherlands.

Karpat, Y.; Özel, T. (2005) Predictive analytical and thermal modeling of orthogonal cutting process—Part I: Predictions of tool forces, stresses, and temperature distributions. *Journal of Manufacturing Science and Engineering*, 128(2): 435–444.

Komanduri, R.; Hou, Z.B. (2001) Thermal modeling of the metal cutting process—Part III: temperature rise distribution due to the combined effects of shear plane heat source and the tool–chip interface frictional heat source. *International Journal of Mechanical Sciences*, 43(1): 89–107.

Kristyanto, B.; Mathew, P.; Arsecularatne, J.A. (2002) Development of a variable flow stress machining theory for aluminium alloys. *Machining Science and Technology: An International Journal*, 6(3): 365–378.

Lalwani, D.I.; Mehta, N.K.; Jain, P.K. (2009) Extension of Oxley's predictive machining theory for Johnson and Cook flow stress model. *Journal of Materials Processing Technology*, 209(12–13): 5305–5312.

Lazoglu, I.; Altintas, Y. (2002) Prediction of tool and chip temperature in continuous and interrupted machining. *International Journal of Machine Tools and Manufacture*, 42(9): 1011–1022.

Lee, E.H.; Shaffer, B.W. (1951) The theory of plasticity applied to a problem of machining. *ASME Journal of Applied Mechanics*, 73: 405–413.

Li, H.; Wang, J. (2012) A cutting forces model for milling Inconel 718 alloy based on a material constitutive law. *Proceedings of the Institution of Mechanical Engineers, Part C: Journal of Mechanical Engineering Science*, 227(8): 1761–1775.

Meyer Jr, H.W.; Kleponis, D.S. (2001) Modeling the high strain rate behavior of titanium undergoing ballistic impact and penetration. *International Journal of Impact Engineering*, 26(1–10): 509–521.

Oxley, P.L.B. (1989) *The Mechanics of Machining: An Analytical Approach to Assessing Machinability*. Ellis Horwood Limited, Chichester, England.

Özel, T.; Zeren, E. (2005) A methodology to determine work material flow stress and tool-chip interfacial friction properties by using analysis of machining. *Journal of Manufacturing Science and Engineering*, 128(1): 119–129.

Sun, S.; Brandt, M.; Dargusch, M.S. (2009) Characteristics of cutting forces and chip formation in machining of titanium alloys. *International Journal of Machine Tools and Manufacture*, 49(7–8): 561–568.

Tay, A.O. (1993) A review of methods of calculating machining temperature. *Journal of Materials Processing Technology*, 36(3): 225–257.

Tay, A.O.; Stevenson, M.G.; de Vahl Davis, G.; Oxley, P.L.B. (1976) A numerical method for calculating temperature distributions in machining, from force and shear angle measurements. *International Journal of Machine Tool Design and Research*, 16(4): 335–349.

Tlusty, G. (2000) *Manufacturing Equipment and Processes*. Prentice-Hall, Upper Saddle River, New Jersey.

APPENDIX

The variation of the shear flow stress across the width of the parallel-sided shear zone is different because of the use of Johnson–Cook material model. It can be evaluated as follows

$$\frac{\Delta k}{\Delta s_2} = \frac{dk}{ds_2} = \frac{dk}{d\gamma}\frac{d\gamma}{dt}\frac{dt}{ds_2} \tag{A1}$$

From Equation (1), it can be obtained at AB that

$$\frac{dk}{d\gamma} = \frac{d\sigma/\sqrt{3}}{\sqrt{3}d\varepsilon} = \frac{nB\varepsilon_{AB}^{n-1}}{\sqrt{3}(A + B\varepsilon_{AB}^{n})}k_{AB} \tag{A2}$$

$$\frac{d\gamma}{dt} = \dot{\gamma}_{AB} = C_0\frac{V_s}{l} \tag{A3}$$

$$\frac{dt}{ds_2} = \frac{1}{U\sin\phi} \tag{A4}$$

Substituting Equations (A2)–(A4) into Equation (A1) yields

$$\frac{\Delta k}{\Delta s_2} = C_0\frac{2k_{AB}nB\varepsilon_{AB}^{n}}{(A + B\varepsilon_{AB}^{n})l} \tag{A5}$$

$$p_A - p_B = \frac{\Delta k}{\Delta s_2}l = C_0\frac{2k_{AB}nB\varepsilon_{AB}^{n}}{(A + B\varepsilon_{AB}^{n})} \tag{A6}$$

In Oxley's theory,

$$\tan\theta = 1 + 2\left(\frac{\pi}{4} - \phi\right) - \frac{\Delta k l}{2k_{AB}\Delta s_2} \tag{A7}$$

Substituting Equation (A5) into Equation (A7) gives

$$\theta = \tan^{-1}\left(1 + 2\left(\frac{\pi}{4} - \phi\right) - C_0\frac{nB\varepsilon_{AB}^n}{A + B\varepsilon_{AB}^n}\right) \tag{A8}$$

Similarly, the tool-chip contact length h and the normal stress σ_N' at point A should also be updated as

$$h = \frac{t_1 \sin\theta}{\cos\lambda \sin\phi}\left\{1 + \frac{C_0\frac{nB\varepsilon_{AB}^n}{A+B\varepsilon_{AB}^n}}{3\left[1 + 2(\frac{\pi}{4} - \phi) - C_0\frac{nB\varepsilon_{AB}^n}{A+B\varepsilon_{AB}^n}\right]}\right\} \tag{A9}$$

$$\sigma_N' = k_{AB}\left(1 + \frac{\pi}{2} - 2\alpha - 2C_0\frac{nB\varepsilon_{AB}^n}{A + B\varepsilon_{AB}^n}\right) \tag{A10}$$